Physical modelling of the circumstellar material in the early-type active binary HH Carinae

H. Bakış,[1][★] D. T. Köseoglu,[1,2] V. Bakış,[1] C. Nitschelm[3] and Z. Eker[1]

[1]*Akdeniz University, Faculty of Science, Department of Space Sciences and Technologies, Kampus, 07058, Konyaaltı, Antalya, Turkey*
[2]*TÜBİTAK National Observatory, 07070 Konyaaltı Antalya, Turkey*
[3]*Centro de Astronomía (CITEVA), Universidad de Antofagasta, Avenida Angamos 601, Antofagasta, Chile*

ABSTRACT

High-resolution spectra ($R \sim 48\,000$) of the massive binary system HH Carinae have been analysed. Precise absolute parameters were derived from a simultaneous solution of the radial velocities and the light curves. The primary component is found to be an O9-type main-sequence star with a temperature of 33 500 K, while the secondary component is a B0-type giant/subgiant star with a temperature of 27 500 K. An analysis of the spectroscopic and photometric data has shown that the primary component rotates at a speed of $v_{\mathrm{rot1}} = 220$ km s^{-1}, which is three times faster than the synchronous rotation, while the secondary component synchronously rotates with the orbit at a speed of $v_{\mathrm{rot2}} = 150$ km s^{-1}. The distance to the system and the velocity of the centre of mass are determined as $d = 4.6 \pm 0.8$ kpc and $V_\gamma = -16$ km s^{-1}, respectively. The distance of the system is in agreement with the most probable *Gaia* distance of $4.9^{+0.9}_{-0.7}$ kpc and the distance in the latest data release (DR3) of 4.4 ± 0.3. Emission structures at the Hα region were modelled using the code SHELLSPEC where the derived absolute parameters of the components have been considered. Because the components are massive stars, mass loss as a result of stellar winds is expected. Produced models confirm that the components do indeed have strong stellar winds and there is mass transfer from the secondary to the primary. Stellar winds and the gas stream between the components have been modelled as a hot shell around the system, with a temperature of $\sim$22 000 K. Models also indicate that the interaction between the wind and the gas stream causes the formation of a high-temperature (100 000 K) impact region.

Key words: accretion, accretions discs – binaries: eclipsing – circumstellar matter – stars: individual: HH Carinae.

1 INTRODUCTION

Significant progress has been made on the investigation of eclipsing and spectroscopic binary systems, especially during the last 20 years, as a result of the development of CCD technology and radial velocity measurement methods, such as multidimensional cross-correlation and separation of components from composite spectra. Therefore, the mass, radius and other stellar parameters can be obtained with high accuracy in many regions of the Hertzsprung–Russell (H–R) diagram. These parameters constrain the theories of stellar evolution and are also used to test them. The investigations in this field by Andersen (1991) give fine details on this scheme. However, the data in some specific regions of the H–R diagram are not of satisfactory sensitivity. One of these regions corresponds to the hottest stars that have O–B spectral types.

The temperatures of these stars are in the range of 15 000–38 000 K, in which the stars of the O and B spectral classes are listed (Hilditch & Bell 1987). At these temperatures, stellar spectra predominantly contain hydrogen Balmer series lines and broadened helium lines. Especially in this temperature range, the lines are affected by the Stark effect. Thus, the lines broadened by both the Stark effect and high rotation may cause problems,

such that important spectral features may be lost within the noise level of the spectrum. Moreover, the broadened line wings can be seen over the other nearby lines. In such cases, the 'line-blending' effect becomes very effective on the spectrum. In the spectra of binary systems, this effect can be detected in two ways. In the first case, the mixing of the two spectral lines is only seen in the spectrum of one component. Although this does not constitute a major problem, it should be examined carefully, especially for stellar chemical abundance analysis. In the second case, the spectral lines of the components are mixed with each other, which could affect the final values of the basic parameters of the components to a non-negligible level. Moreover, the spectral lines that are blended may belong to the same or different elements. This phenomenon is known as the 'pair-blending' effect and this can now be solved with modern analysis techniques, such as spectral disentangling; for Algol type systems, see, for example, Bakış et al. (2006), and for W UMa type systems, see Özkardeş, Erdem & Bakış (2009).

Popper (1980) lists 20 binary systems with detached, semidetached and contact variable systems with components from B5 and earlier spectral types. Only four of these systems could be obtained with a mass accuracy of 15 per cent. Hilditch & Bell (1987) created a new list of 31 systems in total, including the 20 systems that Popper examined. In this study, masses had been determined with 10 per cent error. Andersen (1991) obtained the parameters for only eight systems with sufficient sensitivity. More recently, Vanbeveren & Mennekens
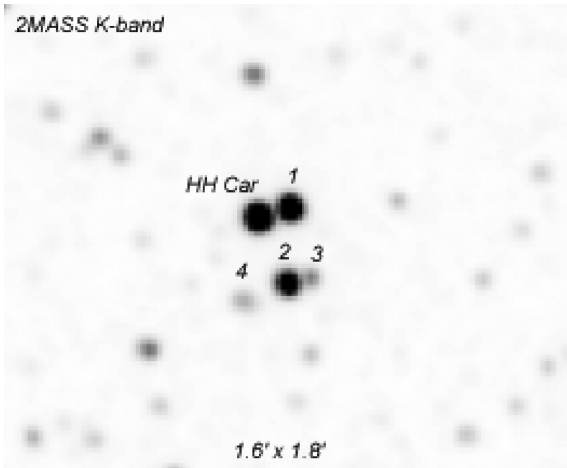
★ E-mail: hicranbakis@akdeniz.edu.tr

Figure 1. The 2MASS (Cutri et al. 2003) *K*-band image of HH Car and other stars in its vicinity. The image dimension is 1.6×1.8 arcmin^2.

(2017) have debated the past and present status of the interacting OB-type binary frequency in their review. Mayer, Drechsel & Irrgang (2014) identified new and improved orbital and stellar parameters of seven OB type binary systems using Fiber-fed Extended Range Optical Spectrograph (FEROS) archive data. Some detailed studies of OB spectral type binary systems have also been made in recent years (Mayer, Lorenz & Drechsel 1997; Caballero 2008; Bakış et al. 2016a, b). In the results, it is obvious that it is necessary to investigate OB-type binary systems and to determine physical parameters, such as mass and radius, with high precision. In order to better understand the evolution of single and binary stars and to explore the physical processes more sensitively, especially in early spectral types, it is very important to study OB-type systems.

HH Carinae (HH Car, HD 303503, $V = 11.49$ mag) is an SB2-type eclipsing binary whose components are of OB type. The system was discovered by O'Connell (1968) at the Riverview College Observatory in Australia. HH Car is accompanied by three visual components, one of which is close to the binary system and the other two are far away according to 796 Riverview photographic plates. However, the photographic plates are not very clear, so the sensitivity in the data is low.

In Fig. 1, we show the positions of the stars using the Two-Micron All-Sky Survey (2MASS; Cutri et al. 2003) *K*-band image in a 1.6×1.8 arcmin^2 box centred on HH Car. The closest visual component (labelled 1) is 6.2 arcsec away, while other two (labelled 2 and 3) are at distances of 13.6 and 14.7 arcsec, respectively. The most distant fourth (4) is at a distance of 16 arcsec.

O'Connell (1968) states that there is a difference of 0.0000281 d between the periods determined by the first and second minima times. This can happen if the system is eccentric and shows an apsidal motion. He used the light elements to determine the rotation period of the line of apsides and made an O – C period analysis of the system. As a result, ~660 yr has been determined as the apsidal motion period. He also calculated the orbital period $P = 3.23$ d, the inclination of orbit $i = 87°.9$ and the eccentricity $e = 0.16$, and gave the Johnson *B*-filter light contributions of the primary and secondary components as 0.546 and 0.454, respectively.

Soderhjelm (1975) obtained a different light curve compared with the light curve of O'Connell. He claimed that the orbit of the binary system is circular and there is no sign of orbital eccentricity. He also stated that the secondary component is larger and brighter but cooler than the primary component. He determined the orbital

period $P = 3.23$ d, orbital inclination $i = 81°.5$ and the mass ratio $q = 0.91$. According to Soderhjelm (1975), the system is in a semidetached configuration, and the O – C analysis indicates that mass transfer occurs between the components. The asymmetry seen in the minima indicates an absorption of the circumstellar matter around the star. The declines in the light curve seen just before and after the conjunctions are linked to the disc-like structures, which are interpreted as a consequence of the mass transfer.

Mandrini et al. (1985) measured the Doppler shifts in the He I lines and found the radial velocity half-amplitudes of the primary and secondary components as $K_1 = 202 \pm 15$ km s^{-1} and $K_2 = 247 \pm 8$ km s^{-1}, respectively, assuming $e = 0$. Soderhjelm (1975) calculated the mass and radius of primary and secondary components as 17 M$_\odot$, 6.1 R$_\odot$ and 14 M$_\odot$, 10.7 R$_\odot$, respectively. The presence of the He II 4541 Å line, which is weaker than the He I 4471 Å line in the spectra and clearly visible only in certain phases, shows that the hotter but smaller and fainter primary component is a main-sequence star of an O8 spectral type.

Based on the strong Si IV and O II lines seen at the primary minimum, where the hot primary is covered by the cooler and larger secondary, the spectral type of the secondary is identified as B0 III. Mandrini et al. (1985) also noted that there is no spectral evidence of the environmental matter in the lines they studied, and therefore the Hα line taken at different epochs had to be inspected by taking high-resolution spectra. Soderhjelm (1975) pointed out that the surface temperature values given as 45 000 K and 38 000 K, respectively, for the primary and secondary components were about 10 000 K higher than the required values. Using spectral lines, authors who obtained the spectra of the brightest visual component in the system have determined that this visual component is an F0-2 II spectral type and moves at 24 ± 5 km s^{-1}. However, they found no strong evidence of the physical connection of the visual component to the system.

In the present study, new and only high-resolution spectroscopic data are used, together with available photometric data from the literature, to determine the complex nature of HH Car.

2 SPECTROSCOPY

Spectroscopic observations of HH Car were performed with the 2.2-m diameter MPG/ESO telescope and the high-resolution, R ($\lambda/\Delta\lambda$) = 48 000, $\Delta\lambda = 0.09$ Å at 4471 Å, FEROS attached to it at the European Southern Observatory (ESO) in La Silla, Chile. The spectroscope acquires the region of the electromagnetic spectrum between approximately 350 and 920 nm wavelengths in a single spectral image with 39 echelle orders. It contains two fibre cables that allow both the star and the sky (flat-field view) or calibration lamps (wavelength calibration) to be observed at the same time. The distance between the areas of these fibre cables seen on the sky plane is 50 arcsec. As the detector, a CCD is used with a size of 2k × 4k of EEV type, which is thinned and back-illuminated. For such CCDs, the quantum efficiency is high, and for FEROS this value is measured as 98 per cent at the 450-nm wavelength (Kaufer et al. 1999). The fibre diameter of FEROS is 2.7 arcsec, so the spectra taken with this instrument are free from the effects of the closest visual component (labelled 1 in Fig. 1) of HH Car.

The data reduction software for FEROS was developed and distributed with the MIDAS software under the name 'feros'. This program can be used to separate echelle orders as well as to clean cosmic rays. Basic steps, such as bias effect extraction, normalization of flat-field image, extraction of echelle orders and wavelength

Table 1. Journal of spectroscopic observations.

No.	Time (HJD)	Date	Phase (ϕ)
1	245 5647.5586	2011.03.27	0.512
2	245 5647.5731	2011.03.27	0.516
3	245 5647.7272	2011.03.27	0.564
4	245 5647.7417	2011.03.27	0.569
5	245 5648.6492	2011.03.28	0.849
6	245 5648.6637	2011.03.28	0.854
7	245 5648.4970	2011.03.28	0.112
8	245 5649.5115	2011.03.29	0.116
9	245 5649.5874	2011.03.29	0.140
10	245 5649.6019	2011.03.29	0.144
11	245 5649.6498	2011.03.29	0.159
12	245 5649.6643	2011.03.29	0.164
13	245 5650.5838	2011.03.30	0.448
14	245 5650.5983	2011.03.30	0.453
15	245 5650.6129	2011.03.30	0.457
16	245 5650.6274	2011.03.30	0.462
17	245 5650.6423	2011.03.30	0.466
18	245 5650.6568	2011.03.30	0.471
19	245 5650.6713	2011.03.30	0.475
20	245 5650.6859	2011.03.30	0.480
21	245 5651.5233	2011.03.31	0.739
22	245 5651.5378	2011.03.31	0.743

calibration, were performed with this software during the reduction of the spectra.[1]

A total of 22 spectra of HH Car were collected in 2011 March with FEROS at La Silla (Bakış et al. 2015). The exposure time for each spectrum is 1200 s. The journal of spectroscopic observations is given in Table 1. The phases are calculated using the light elements, which were obtained from the spectroscopic orbital solution (see Table 5).

In order to precisely determine the signal-to-noise (S/N) ratios on a spectrum, spectral regions that are unaffected by emission or absorption, and that have not been affected by cosmic rays or bad pixels on the CCD, must be selected. Accordingly, the average S/N ratios of the spectra of HH Car at 4000, 5000, 6000, 7000 and 8000 Å were calculated as 46, 94, 114, 113 and 94, respectively.

The prominent spectral lines have been determined and spectral regions including these prominent lines have been generated with 30–20 Å wavelength intervals. In Table 2, the visible spectral lines are listed for reference.

2.1 Spectroscopic orbit

The blending of lines of early spectral type stars with high rotational velocities occurs among the hydrogen lines more than in the helium and other metallic lines (Petrie, Andrews & Scarfe 1967). At the same time, line blending is more visible on the helium lines than on the metallic lines (Hilditch 1973). This blending effect seen in the same spectral lines was studied theoretically in detail by Tatum (1968). As a result, this effect was found to be related to the ratio of the linewidths to the spectral line separation of the components. If the blending effect dominates, the amplitude of the radial velocity is measured to be smaller than what it is supposed to be. For this reason, lower mass values are found (Petrie et al. 1967). In Andersen, Clausen & Nordstrom (1980), for stars between O8 and A8 spectral types, the component masses were found to be 10 per cent smaller by

measuring from helium lines, while the masses were determined to be 40 per cent smaller by the hydrogen Balmer lines. Therefore, the main reason for the high uncertainty in the masses of stars in early-type binary systems is the inaccurate radial velocity measurement due to the blending of the lines.

In the spectra of HH Car, the lines of both components can be easily identified. Besides the Doppler shift of the relatively strong Balmer and helium lines, the strong emission and broadened structure of the H_α line of both components draw attention. Because the hydrogen lines show emission and the metal lines are too shallow, the helium lines with relatively weaker emission are used in the radial velocity measurements of HH Car.

Radial velocity measurements were made using two different methods with wavelength calibrated and normalized spectra: Gaussian profile fitting to line centres and disentangling the components' spectra. The use of two independent methods to measure radial velocities is important in terms of checking the measurements. Radial velocity measurements were first made by fitting a Gaussian profile to He I lines at 4026 Å, 4387 Å, 4471 Å, 5875 Å and 6678 Å wavelengths. This is done using the 'deblend' function in the 'splot' task in IRAF.[2] The radial velocity curve of the components was then obtained with the radial velocity values and their uncertainties corresponding to each spectral phase. Using radial velocities determined for each spectral line, orbital solutions are obtained by applying the downhill simplex (Nelder & Mead 1965) algorithm. From each data set, the orbital parameters are obtained and they are averaged to be used as input for the next method of radial measurement and spectroscopic orbit modelling, namely, spectral disentangling with KOREL[3] (Hadrava 2004). According to the preliminary solution, the orbital parameters are $K_1 = 150 \pm 18$ km s^{-1}, $K_2 = 283 \pm 20$ km s^{-1}, $e = 0.02 \pm 0.04$, $w = 103 \pm 11$, $V_\gamma = -20 \pm 7$ km s^{-1} with an averaged rms of 41 km s^{-1}. Relatively high rms and parameter uncertainties are estimated to be the result of emission in the lines. This is later compensated by the modern analysis technique of spectral disentangling.

Using the light contributions of the components, the code KOREL disentangles the component spectra in the Fourier domain and solves the spectroscopic orbit. If light contributions are not available, only the orbital solution can be done. Therefore, selection of orbital parameters for convergence is needed. The orbital period of the system is best known from the photometry (Kreiner 2004) and it cannot be obtained better with 22 radial velocities distributed in one orbital cycle. Thus, the orbital period P is fixed. Although orbital eccentricity seems spurious with its small value and relatively large uncertainty, it is set as a free parameter similar to other parameters such as ephemeris time T_0, periastron longitude ω, radial velocity semi-amplitude of the primary component K_1 and mass ratio q. The spectral disentangling applied to 12 different wavelength regions is summarized in Table 3. Before starting the solutions with KOREL, the light curves of the system should be analysed and the light contributions of the components should be determined. For this purpose, the light curves of HH Car obtained by Soderhjelm (1975) on the U, B, V filters were analysed to determine the light contributions of the components at the relevant wavelengths and the phases of the spectra. For each region, the parameters are converged and the orbital eccentricity converged to zero, implying a circular

---

[1]https://www.eso.org/sci/facilities/lasilla/instruments/feros/tools/DRS.html

[2]IRAF is distributed by the National Optical Astronomy Observatories, which are operated by the Association of Universities for Research in Astronomy, Inc., under cooperative agreement with the National Science Foundation.
[3]https://stelweb.asu.caz.cz/vo-korel/

Table 2. Visible spectral lines in the spectra of HH Car.

Order	Spectral region (Å)	Range $(\Delta\lambda)$	Lines
1	3872–3902	30	3889 He I, 3889 H_ζ
2	4010–4041	31	4026 He I
3	4065–4187	122	4088–4116 Si IV, 4101 H_δ, 4120–4143 He I
4	4305–4367	62	4340 H_γ, 4317–4348 O II
5	4367–4400	33	4379 N III, 4388 He I
6	4400–4461	61	4416–4447 O II
7	4456–4487	31	4471 He I, 4481 Mg II
8	4528–4590	62	4541 He II, 4552–4567–4574 Si III
9	4628–4690	62	4640 N III, 4650 C III III, 4661-4676 O II, 4686 He II
10	4700–4761	61	4713 He I
11	4829–4891	62	4861 H_β
12	4904–4935	31	4921 He I
13	5000–5062	62	5015, 5048 He I
14	5853–5885	32	5875 He I
15	6540–6590	50	6563 H_α
16	6660–6692	32	6678 He I
17	7030–7090	60	7064 He I

Table 3. Results of the KOREL analysis for different spectral regions for HH Car.

Spectral region (Å)	T_0 (HJD)	K_1 (km s^{-1})	K_2 (km s^{-1})	q (K_1/K_2)
3872–3902	245 2501.6406	158.2	253.9	0.623
4065–4187	245 2501.6407	164.8	263.0	0.627
4305–4367	245 2501.6396	156.4	258.6	0.605
4367–4400	245 2501.6401	160.7	263.9	0.609
4400–4461	245 2501.6399	160.3	268.5	0.597
4456–4487	245 2501.6390	165.1	266.6	0.619
4528–4590	245 2501.6400	165.5	285.8	0.579
4628–4690	245 2501.6385	151.9	273.5	0.555
4700–4761	245 2501.6398	161.0	271.1	0.594
4904–4935	245 2501.6407	163.3	263.5	0.620
5000–5062	245 2501.6399	164.9	281.2	0.586
6660–6692	245 2501.6400	158.8	268.2	0.592

Table 4. Radial velocities of the components of HH Car.

HJD	Phase (ϕ)	RV_1 (km s^{-1})	$O - C_1$ (km s^{-1})	RV_2 (km s^{-1})	$O - C_2$ (km s^{-1})
245 5647.5586	0.512	−3.8	−0.5	−36.5	0.0
245 5647.5731	0.516	2	0.6	−44.5	−0.5
245 5647.7272	0.564	49.1	0	−121.8	−0.8
245 5647.7417	0.569	53.5	0.2	−128.3	−0.4
245 5648.6492	0.849	118.2	0.5	−231.6	0.4
245 5648.6637	0.854	114.5	−0.4	−227.5	0.0
245 5649.497	0.112	−122.9	0	156.6	−0.1
245 5649.5115	0.116	−126.5	−0.1	161.9	−0.4
245 5649.5874	0.14	−143.8	−0.5	189.6	0.1
245 5649.6019	0.144	−146.5	−0.3	193.8	−0.5
245 5649.6498	0.159	−155.6	−0.5	208.9	0.3
245 5649.6643	0.164	−157.1	0.4	213	0.4
245 5650.5838	0.448	−68.9	−0.4	69.4	0.5
245 5650.5983	0.453	−63.7	0.4	61.8	0.1
245 5650.6129	0.457	−59.5	0.1	54	−0.4
245 5650.6274	0.462	−54.8	0.3	47.1	−0.1
245 5650.6423	0.466	−49.8	0.6	39.8	0.2
245 5650.6568	0.471	−46.2	−0.3	33	0.7
245 5650.6713	0.475	−41.4	−0.1	24.8	−0.1
245 5650.6859	0.48	−36.6	0	17.4	0.0
245 5651.5233	0.739	147.1	−1.6	−281.7	0.3
245 5651.5378	0.743	148.9	0	−282.1	0.3

orbit. This is expected because the system is semidetached and highly interacting, which causes the orbit to quickly circularize (Zahn 1977).

The measured radial velocities of the components and the final orbital solution parameters of the system are given in Tables 4 and 5, respectively. In addition, the radial velocities for the components and the best-fitting curves are shown in Fig. 2.

Table 5. Final set of parameters for the spectroscopic orbit.

Parameter	Values
P (d)	3.231515
T_0 (HJD 245 2501)	0.64 ± 0.01
K_1 (km s^{-1})	161 ± 4
K_2 (km s^{-1})	268 ± 9
e	0
V_γ (km s^{-1})	-16 ± 3
$q(M_2/M_1)$	0.60 ± 0.04
$m_1\sin^3 i$ (M$_\odot$)	16.5 ± 1.6
$m_2\sin^3 i$ (M$_\odot$)	9.9 ± 0.9
$a \sin i$ (R$_\odot$)	27.4 ± 0.8

2.2 Stellar atmosphere models

In the last decades, stellar atmosphere models have become a key tool in understanding massive stars. Because HH Car consists of OB spectral type components, which have high surface temperatures, we prefer the model atmosphere codes using the non-local thermodynamic equilibrium (NLTE) approach to the calculation of the atmosphere parameters of the components. The OSTAR2002 catalogue was used to construct the model atmospheres of the HH Car system (Lanz & Hubeny 2003). The atmospheric grids in this catalogue are calculated with the TLUSTY code to form the model atmospheres and the SYNSPEC code to produce the synthetic spectrum. In addition, the model atmosphere grids with solar abundance were prepared at a wavelength range of 300–750 nm, at a temperature range of 27500–55 000 K with increments of 2500 K, and at a gravitational acceleration, log g, range of 3.00–4.75 with increments of 0.25.
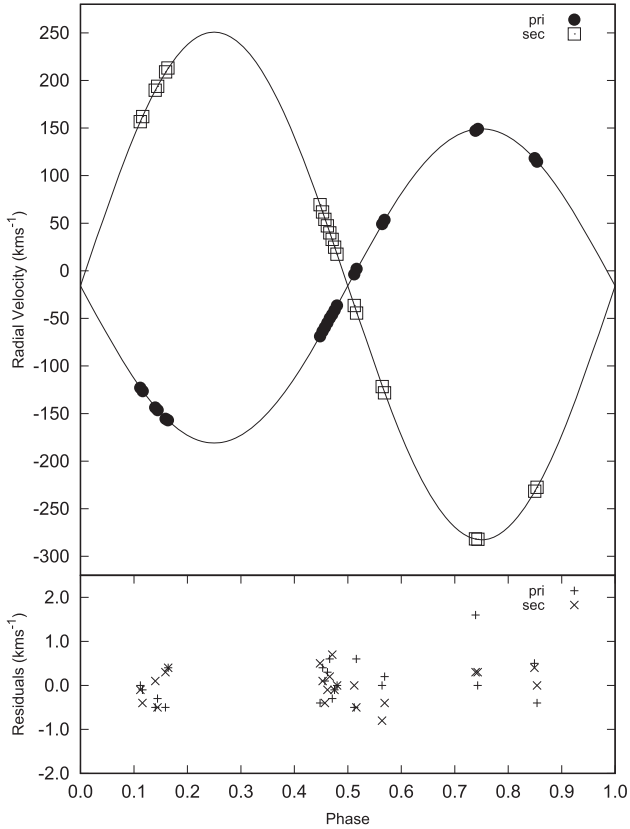
Figure 2. Spectroscopic orbital solution.

Except for the visible region, detailed model atmospheres of the ultraviolet region between 90 and 200 nm are also available in the same catalogue. Because the OSTAR2002 model atmospheric grids are calculated based on the assumption that the rotation speed of stars is zero, the ROTIN3 code[4] is used to generate the synthetic spectra from which the rotation is considered.

The disentangled spectra of the components of HH Car were obtained by KOREL, taking into account the light contributions of the components. Disentangled lines of the primary are broadened due to rapid rotation. Emission due to the gas stream and winds cause observed line asymmetries. Indeed, strong emissions seen in both helium and metallic lines indicate how strong the mass transfer activity is. For this reason, synthetic spectra of the primary are produced to estimate only the rotational speed. A projected rotational velocity, $v \sin i_1 = 220 \pm 30$ km s^{-1} was determined for this component. The disentangled lines of the secondary component appear to be more symmetric. Therefore, atmospheric parameters and rotational speed were easily determined for the secondary. The model atmospheres and synthetic spectra are calculated by using solar abundance ([M/H] $= 0$ dex) and the velocity of microturbulence, ζ, as 10 km s^{-1}. The rest of the parameters were found to be the following: effective temperature of the secondary component $T_{\rm eff2}$ $= 27\,500$ K, the surface gravity acceleration $\log g = 3.50$ cgs, and the projected rotational velocity $v \sin i_2 = 150 \pm 5$ km s^{-1}. Fig. 3 shows the best fits to the disentangled spectra of the secondary in four different spectral regions.

[4]http://nova.astro.umd.edu/Synspec49/synspec-frames-guides.html

3 ANALYSIS OF THE PHOTOMETRIC DATA

The light-curve solution of the HH Car binary system has been utilized using the 2007 version of the Wilson–Devinney (WD) code (Wilson 2008). Because emissions on its spectra indicate mass transfer or accretion, mod 5 is chosen for analysis in the WD code. Observations on Johnson *U*, *B*, *V* filters are taken from Soderhjelm (1975). The orbital period *P* and the ephemeris time T_0 of the system are taken from Kreiner (2004), where *P* is fixed and T_0 is left to converge. The semimajor axis and mass ratio obtained from the KOREL code are taken as fixed values in the analysis. The surface potential values of the secondary component are also kept constant. The initial value of the inclination of the system was taken from Soderhjelm (1975) as 81°.5 and left free.

In the light-curve analysis, one of the most critical parameters is the temperature of one of the components as the light-curve analysis gives the temperature ratio of the components. In Section 4, a reliable temperature determination has been made, that is, the temperature of the secondary component can be used in the analysis of the light-curve data. For both components, the gravitational darkening (g_1, g_2) and albedo (A_1, A_2) are taken as 1.0 for the radiative stars and are fixed during the iterations. The synchronized rotational parameter of the components ($F_{1,2} = v_{\rm rot1,2}/v_{\rm synch1,2}$) was initially set to 1.0 because the radii of the components were not known. Once the synchronous rotation velocity of the components are calculated from the light-curve model parameters, the actual values of the synchronized rotational parameter are found for each component as $F_1 = 2.9$ and $F_1 = 1.0$ using the rotational speed of the components ($v \sin i_1 = 220 \pm 30$ km s^{-1} and $v \sin i_2 = 150 \pm 5$ km s^{-1}) (see Section 2.2). The logarithmic limb darkening coefficients were calculated by interpolation from the Claret (2000) table. Soderhjelm (1975) states that his light curve is free from the effects of the visual components around HH Car. Therefore, no third light contribution has been assumed. The final light-curve model parameters with their uncertainties are given in Table 6 and the best-fitting light curves are shown in Fig. 4 together with the observational data. As the system is semidetached, only the primary component's surface potential (Ω_1) is converged as a free parameter and the secondary component's surface potential (Ω_2) is determined by the system mass ratio and it is fixed during the solutions. Therefore, the mean relative radius of the components ($r_{1,2}$) are determined from the final values of the surface potentials. The geometric view of the components is shown in Fig. 5.

In order to check the results, the Q-method given by Johnson & Morgan (1953) has been used to calculate the surface temperature of the primary component, $T_{\rm eff1}$. Soderhjelm (1975) gave ($U - B$) and ($B - V$) colours for the primary component as –0.68 and 0.27 mag, respectively. With the Q-method, the unreddened colours are calculated as –1.093 and –0.304 mag for ($U - B$)$_0$ and ($B - V$)$_0$, respectively. Based on the colour–temperature calibration tables given by Worthey & Lee (2011), these colour values give a surface temperature of 32 000 K for the primary component, which is in good agreement with the value obtained in the light-curve analysis.

4 ASTROPHYSICAL PARAMETERS AND THE DISTANCE OF THE SYSTEM

The absolute parameters from the simultaneous solution of the light and radial velocity curves are summarized in Table 7. According to Table 7, the separation between the components is 27.8 R$_\odot$ and the masses of the components for the primary and secondary are 17 M$_\odot$ and 10 M$_\odot$, respectively. Using calibration tables of Straizys & Kuriliene (1981), the masses of the components are suitable for
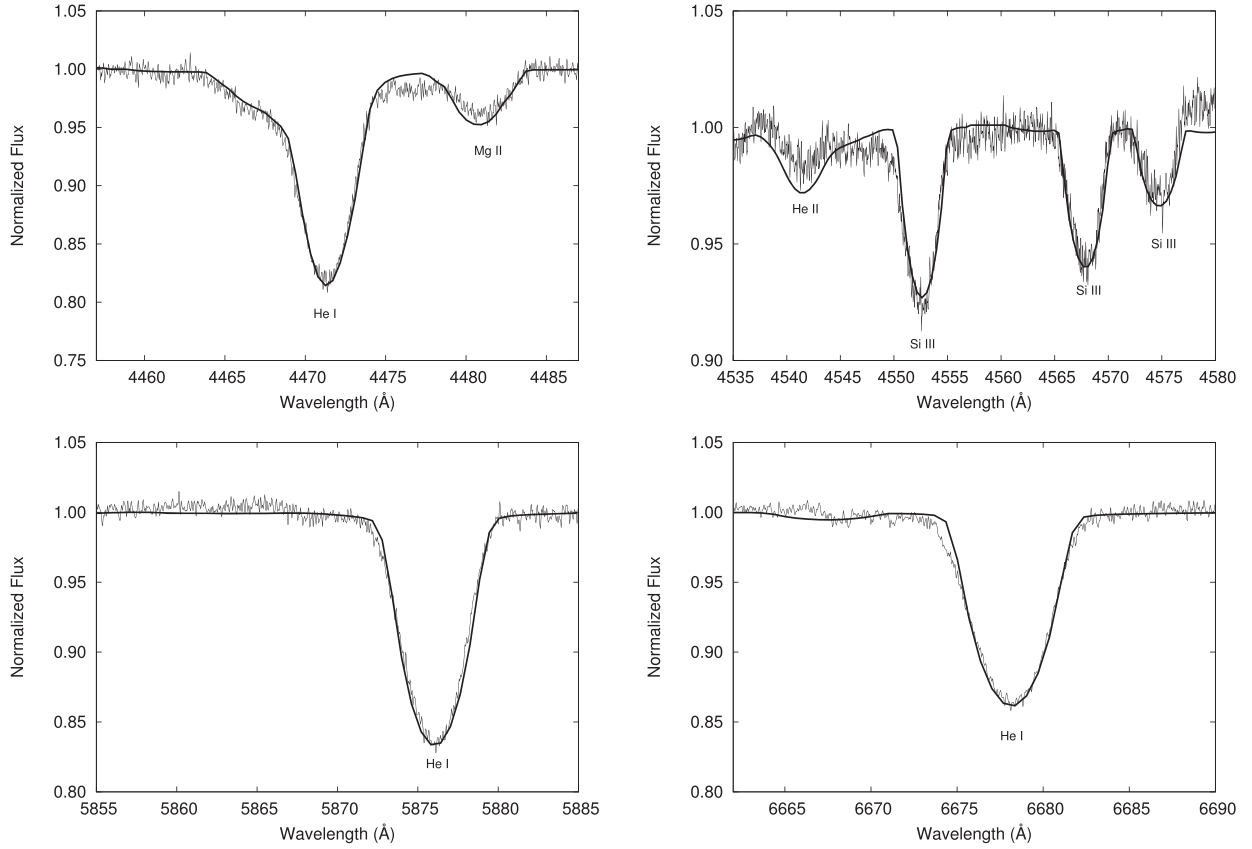
Figure 3. Synthetic spectra fitted to the disentangled spectrum of the secondary. The model atmosphere is indicated by the solid line.

Table 6. Results from the simultaneous solution of multiband light curves of HH Car. Errors refer to program outputs.

Parameter	Value	Error
P (d)	3.231515	
T_0 (HJD 245 2501)	0.6400	0.0008
T_{eff1} (K)	33 500	100
T_{eff2} (K)	27 500	
q	0.60	0.04
L_1/L_{1+2} (U)	0.28	0.01
L_1/L_{1+2} (B)	0.27	0.01
L_1/L_{1+2} (V)	0.26	0.01
e	0.0	
w $(°)$	0.0	
i $(°)$	80.9	0.1
F_1	2.9	
F_2	1.0	
Ω_1	6.301	0.022
Ω_2	3.021	
r_1	0.175	0.001
r_2	0.337	0.001
χ^2 (U, B, V)	0.08, 0.11, 0.11	

spectral types B0 V and B2 IV–III for the primary and secondary, respectively. The radii of the stars were found to be 4.86 $R_\odot$ and 9.35 $R_\odot$ for the primary and the secondary, respectively. These radii indicate B2 V spectral type for the primary and B0 IV–III for the secondary. However, both of the components have the He II line in their spectra. The existence of the He II line indicates that these components must be of B0 or O spectral type (Gray & Corbally 2009). The spectral types from the temperatures of the primary and secondary components of HH Car were adopted as O9 V and B0 IV–III, respectively. Therefore, determining spectral types from component masses in systems where such mass transfer occurs may lead to incorrect results. The fact that spectral types differ according to mass, radius and temperature is an expected result in semidetached systems, especially in mass-transferring systems. The mass transfer leads to a deviation of the evolution of stars in the binary system from the evolution of a single star. For this reason, the primary component in the H–R diagram appears to be less luminous according to its mass, while the secondary appears to be more luminous (Ibanoğlu et al. 2006).

The unreddened colours of the system $(U − B)_0 = −1.093$ mag and $(B − V)_0 = –0.304$ mag indicate the $E(B − V)$ colour excess of 0.574 mag. The interstellar extinction in the V band is given as $A_V = R \times E(B − V)$. The coefficient R for the direction of the Carina–Centaurus region is studied by Loden & Sundman (1972) and very different R values ranging between 2.1 and 3.5 are determined in a small (2 deg²) region around HH Car. Averaging these values yields $R = 3.0 \pm 0.8$ and implies an extinction of $A_V = 1.722$ mag. Now this value can be used in the distance modulus. The other unknown parameters, such as the absolute magnitudes of the components, are derived from the calculated bolometric magnitudes and bolometric corrections taken from Budding & Demircan (2007), which are given in Table 7. With these values, the photometric distance is calculated to be 4654 ± 795 pc. The distance of HH Car in the *Gaia* DR2 catalogue (Gaia Collaboration 2018) is given as $d_{Gaia} = 5903 \pm 1000$ pc. In addition, the study of Bailer-Jones et al. (2018) updated the released *Gaia* distance with most probable distances, and in their catalogue HH Car is reported to be at a distance of 4875^{+915}_{-680} pc. Moreover,
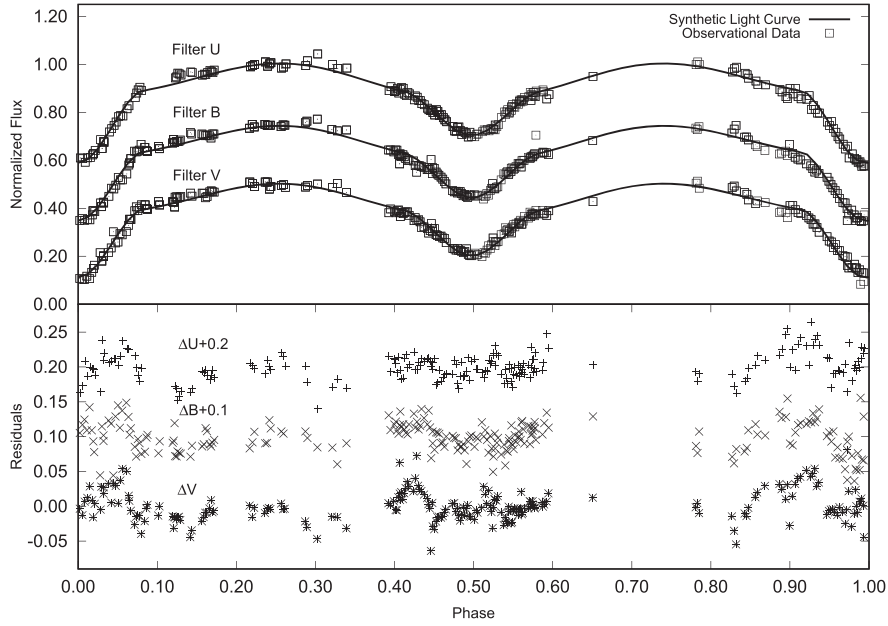
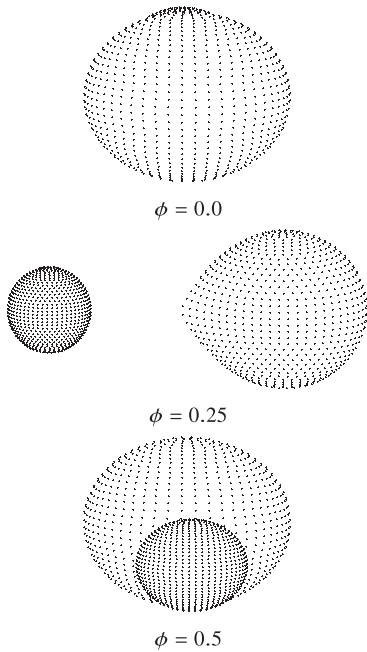**Figure 4.** Best-fitting synthetic light curves.

Figure 5. The Roche equipotentials for the components of HH Car.

an early data release (DR3) of *Gaia* has recently been released and is available in the *Gaia* archive. In DR3, the distance to HH Car is given as $d_{Gaia} = 4398 \pm 266$ pc, which is the most precise reported distance so far for HH Car and is in good agreement with our distance estimation within the uncertainty box.

5 OB ASSOCIATION MEMBERSHIP

HH Car is a massive early-type binary. Therefore, it is a young system and is expected to be related to nearby stellar associations. A possible membership of HH Car to the Car OB1/OB2 association was also

investigated in this study. The Car OB1 association is located at 2.5 kpc and has an average radial velocity of –5 km s^{-1} (Mel'Nik & Dambis [2009]). Also, Mel'Nik & Efremov ([1995]) divide the Car OB1 region into five groups at distances ranging from 2.2 to 2.8 kpc and radial velocities ranging from –16 to 8.2 km s^{-1}. Tetzlaff et al. ([2010]) determined the space velocity components for Car OB1 and OB2 associations as $(U, V, W) = (-66 \pm 1.0, -15.0 \pm 1.6, -8.9 \pm 0.9)$ and $(U, V, W) = (-78.9 \pm 2.4, -25.1 \pm 2.3, -9.7 \pm 2.4)$ km s^{-1}, respectively. Kinematic analysis of the HH Car system has been done to determine its relationship with Car OB1 or Car OB2 associations. The space velocity of components and its errors were calculated using the Johnson & Soderblom ([1987]) algorithm, which takes into account the equatorial coordinates, proper motion components, centre of mass velocity and distance of the system. For this purpose, the proper motion components of the system given in Table [7] are taken from the *Gaia* catalogue (Gaia Collaboration [2018]). The photometric distance and centre of mass velocity of HH Car are calculated as 4.5 kpc and –16 km s^{-1}, respectively. The space velocity components and their errors are calculated as $(U, V, W) = (-124.36 \pm 16.31, -3.72 \pm 1.37, -24.65 \pm 5.53)$ km s^{-1}. Comparing these findings with the parameters of Car OB1 and OB2 given above, HH Car does not seem to be related to one of these associations within the error limits. The system is possibly a member of an undiscovered stellar association that is further than Car OB1 and OB2.

6 MASS TRANSFER AND STELLAR WINDS

Modelling of the emission and absorption features in Balmer lines in the spectra of stars, star formation regions and nebulae is one of the most commonly used methods to study the morphology of these regions. This method is also used to study the distribution of environmental gas and the accretion discs in the stars. The spectral evidence of the circumstellar matter surrounding the components of HH Car is clearly seen in the spectra, particularly in the Hα line profiles. Looking at the spectra of HH Car, a double-peak emission

Table 7. Close binary stellar parameters of HH Car. Errors of parameters are given in parentheses.

Parameter	Symbol	Primary	Secondary
Spectral type	Sp	O9 V	B0 III–IV
Mass ($M_\odot$)	M	17.2 (1.2)	10.3 (0.9)
Radius ($R_\odot$)	R	4.86 (0.18)	9.35 (0.31)
Separation ($R_\odot$)	a	27.8 (0.9)	
Orbital period (d)	P	3.231515	
Orbital inclination ($°$)	i	80.90 (0.09)	
Mass ratio	q	0.600 (0.035)	
Eccentricity	e	0.0 (fixed)	
Surface gravity (cgs)	$\log g$	4.30 (0.06)	3.51 (0.07)
Combined visual magnitude (mag)	V	10.5	
Individual visual magnitudes (mag)	$V_{1,2}$	11.96 (0.07)	10.83 (0.04)
Combined colour index (mag)	$B - V$	−0.304 (0.01)	
Temperature (K)	T_{eff}	33 500 (2500)	27 500 (2500)
Luminosity ($L_\odot$)	$\log L$	4.347 (0.052)	4.574 (0.036)
Bolometric magnitude (mag)	M_{bol}	−6.32 (0.15)	−6.90 (0.23)
Absolute visual magnitude (mag)	M_{v}	−3.10 (0.19)	−4.24 (0.88)
Bolometric correction (mag)	BC	−3.22 (0.05)	−2.65 (0.09)
Velocity amplitudes (km s^{-1})	$K_{1,2}$	161 (4)	268 (9)
Systemic velocity (km s^{-1})	V_γ	−15.9 (3.0)	
Computed synchronization velocities (km s^{-1})	V_{synch}	76 (2)	147 (4)
Observed rotational velocities (km s^{-1})	V_{rot}	220 (30)	150 (5)
Distance (pc)	d	4654 (795)	
Proper motion (mas yr^{-1})	$\mu_\alpha * \cos(\delta), \mu_\delta$	−5.32 (0.06), 2.40 (0.06)	
Space velocities (km s^{-1})	U, V, W	−124.36 (16.31), −3.72 (1.37), −24.65 (5.53)	

is clearly seen and, in some phases, it has an absorption feature accompanying this emission (see Fig. 7).

The double-peak emission in Hα indicates a large disc or shell structure surrounding one or both of the component stars. Models can be made by examining these double-peak structures observed in the shell stars and can be used to calculate the basic parameters such as expansion velocity, density and temperature of the shell. There are extensive studies in the literature about Hα line profiles observed in systems with OB-type components where stellar winds are dominant, in shell stars, 'B$_\text{e}$' spectral type stars and in Algol-type binary systems (Petrenz & Puls 1996; Thaller 1997; Richards & Albright 1999; Nemravová et al. 2010; Richardson et al. 2010; Silaj et al. 2010). According to the result of the light curve analysis of HH Car, the secondary component has filled the Roche lobe and it transfers material to the primary component. For such systems, how the accretion can form around the main component can be estimated from the location of the system in the r_1–q diagram (Lubow & Shu 1975; Peters 1989), where r_1 is the fractional radius of the primary component and q is the mass ratio of the components (M_2/M_1). In this diagram, the ω_d and ω_{min} lines are calculated by Lubow & Shu (1975) for different mass ratio values. The area between these two curves includes systems showing transient disc structures. In the region below the ω_{min} curve, there are systems with permanent discs; the distance between the components of these systems is large and the fractional radius of the mass gainer component is small. For this reason, the gas flow can form a permanent disc. However, in systems located above the ω_d line, the distance between the components is small and the fractional radius of the mass gainer component is very large. The gas flow therefore directly strikes on the surface of the mass gainer component and forms a hot zone there. HH Car is located in the region where the permanent disc structure is not visible and the gas stream directly hits the primary component. Fig. 6 shows the r_1–q diagram and the location of HH Car in this diagram. In addition, HH Car is a system with components of early spectral type (O9 V + B0 IV–III). In such stars, radiatively driven stellar winds

are important. Radiation pressure may cause high-speed supersonic winds that exceed the speed of sound in early spectral type stars. In such systems, the stellar winds of the components interact with each other. Therefore, the effect of the gas stream and the total effect of the stellar winds of the components must also be considered. HH Car is one of these systems.

The code SHELLSPEC (Budaj & Richards 2004) was used in the modelling of the environmental matter in HH Car. In the application of the code, the mass, radius, rotational speeds, temperatures, mass ratio, distance and inclination of the system obtained in this study were used as input parameters. As the mass transfer from the secondary to the primary is known, the gas stream modelling has been activated and it has been assumed that this gas stream has a hot strike region. Mass loss with stellar winds is possible for both components, and the winds of these components can interact with each other. Therefore, it is expected that the gas stream and the interacting stellar winds will form a high-temperature zone between the component stars (e.g. Stevens, Blondin & Pollock 1992). The winds from the components were considered to be a shell expanding around the system, and the shell structure was modelled with different density and thickness values. In the analysis, the SHELLSPEC code uses the ishell = 2 mode, in which the velocity and density quantities of the shell are variable.

The model of HH Car was formed by taking into account the stellar wind from the components and this wind exists in all directions so there must be a shell-like structure. Furthermore, the region between the components must be highly active because the stellar winds and the transferred matter from the secondary component through the first Lagrangian point interact with each other. The assumption here is that this interaction creates a high-temperature region in this area. It has been found that there is a small difference in the temperature, density and the rate of expansion through the shell. This indicates that the expanding shell structure is not homogeneous by the influence of the stellar winds from both components, and that there may be different densities in different regions of the shell
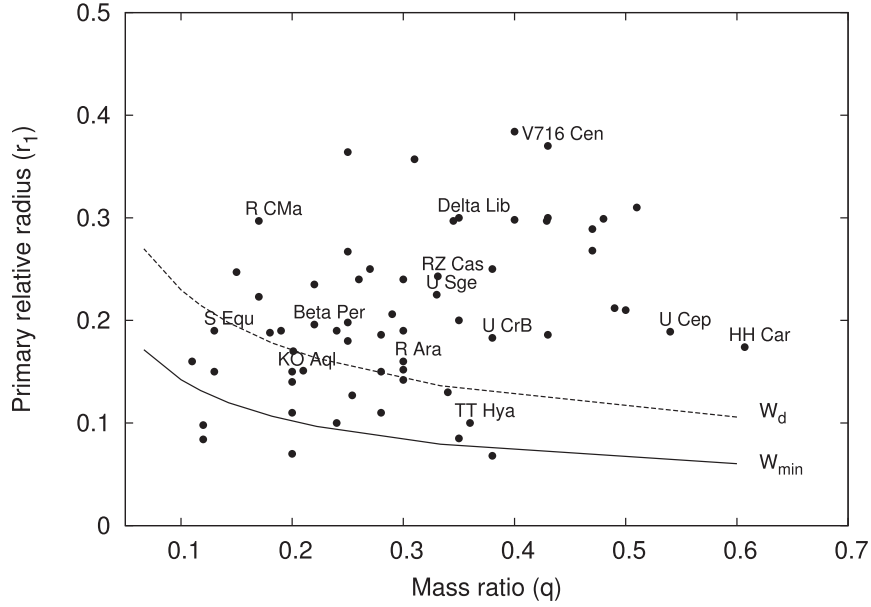
Figure 6. The r_1-q diagram for known Algol systems. Note that HH Car is located above the ω_d curve.

(see Owocki & Rybicki 1984). Fig. 7 shows the synthetic spectra of the Hα region of HH Car generated by the SHELLSPEC modelling. The difference between the two different shell models in which the hotspot is included (shell + spot) and not included (shell) is clearly visible. From Fig. 7, in almost all phases, although the double-peak emission structure has been generally modelled in synthetic spectra, the heights of V and R emissions of the emission line are not properly modelled. This situation is from the assumption that the surrounding material is a spherical shell. However, adding a hot region with a temperature of 100 000 K to the models has been seen to improve the model fits over the observed spectra. In Fig. 7, a binary spectrum model with the shell and hot region is shown together with models with only the shell. Here, the code SHELLSPEC assumes a spherical gas volume for the hot region. However, the structure is not as simple as considered by SHELLSPEC. Stevens et al. (1992) studied the dynamics of the wind and shock structure formed by the wind collision. What we have to ask here is, can such a hot region in HH Car show itself in X-rays? This is a relatively difficult question in our case as the equations require more parameters than we know (see Stevens et al. 1992). For example, the luminosity is strongly correlated with the stellar wind velocity from each component separately. However, in the case of close binaries with short orbital periods, the wind luminosity equation is simplified as

$$L \approx f \dot{M} v^2, \tag{1}$$

where f is the fraction of the wind luminosity lost in the wind shock, $\dot{M}$ is the mass-loss rate and v is the wind speed. We can adopt $f = 1/6$ for the case of equal winds. $\dot{M}$ is calculated in Section 7 using equation (2). We adopted the wind speed as the expansion velocity of the gas (192.5 km s^{-1}) in our model. Using equation (1), the luminosity of the colliding wind is found to be 4×10^{33} erg s^{-1}, which is of the order of L$_\odot$ and can be ignored in the vicinity of two early-type massive stars with luminosities of $L_1 = 22\,233$ L$_\odot$ and $L_2 = 37\,497$ L$_\odot$ (see Table 7). The model parameters obtained for the shell and hotspot region are given in Table 8.

The light curve of the system shows that there are absorptions and emissions. In order to determine how the absorbing matter diffuses,

the differences between the synthetic model and the observational data in the light curves were examined. The optical depth of the circumstellar matter around the system can be found from the expression $\tau = I/I_0$, where I is the observational normalized flux and I_0 is the normalized flux of the model. In addition, the geometric depth, x, can be found using the equation $\tau = aNx$. In the literature, the value of the electron density N parameter for the discs of Algol-type systems and the electron absorption coefficient, a, are given as 10^{10}–10^{11} cm^{-3} (Kaitchuck & Honeycutt 1982; Budaj, Richards & Miller 2005) and 6.654×10^{-25} cm^2, respectively. When the geometric size of the circumstellar matter around the system is determined by taking $aN = 10^{-14}$ cm^{-1} for HH Car, the presence of a absorbing matter going to distances of approximately 35–40 R$_\odot$ is seen. This value is in agreement with the value found from the spectral analysis. Furthermore, Fig. 8, which shows the distribution of the material surrounding the system, shows that absorption is predominant, particularly during the eclipse phases. The spectra of the system indicate the presence of a very hot region between the components. This hot region is seen as excess brightness, except for eclipses in the light curve.

7 CONCLUDING REMARKS

In this study, the high-resolution spectra of HH Car, obtained from the ESO observatory, were analysed together with the multiband light curves, and accurate astrophysical parameters of the system were determined. Reliable astrophysical parameters of the system have enabled the modelling the emissions seen in the spectra.

From the spectra, both the orbital parameters of the system and the disentangled spectra of the components were obtained. Because the components of HH Car are of early-type stars with high effective temperatures, the NLTE approach was used to construct model atmospheres and synthetic spectra of disentangled spectra of the components. Because the spectral lines of the primary component are broadened due to fast rotation and were affected by emission, the synthetic spectra were formed only to determine the rotation speed of this component. As a result, the rotational velocity of the primary
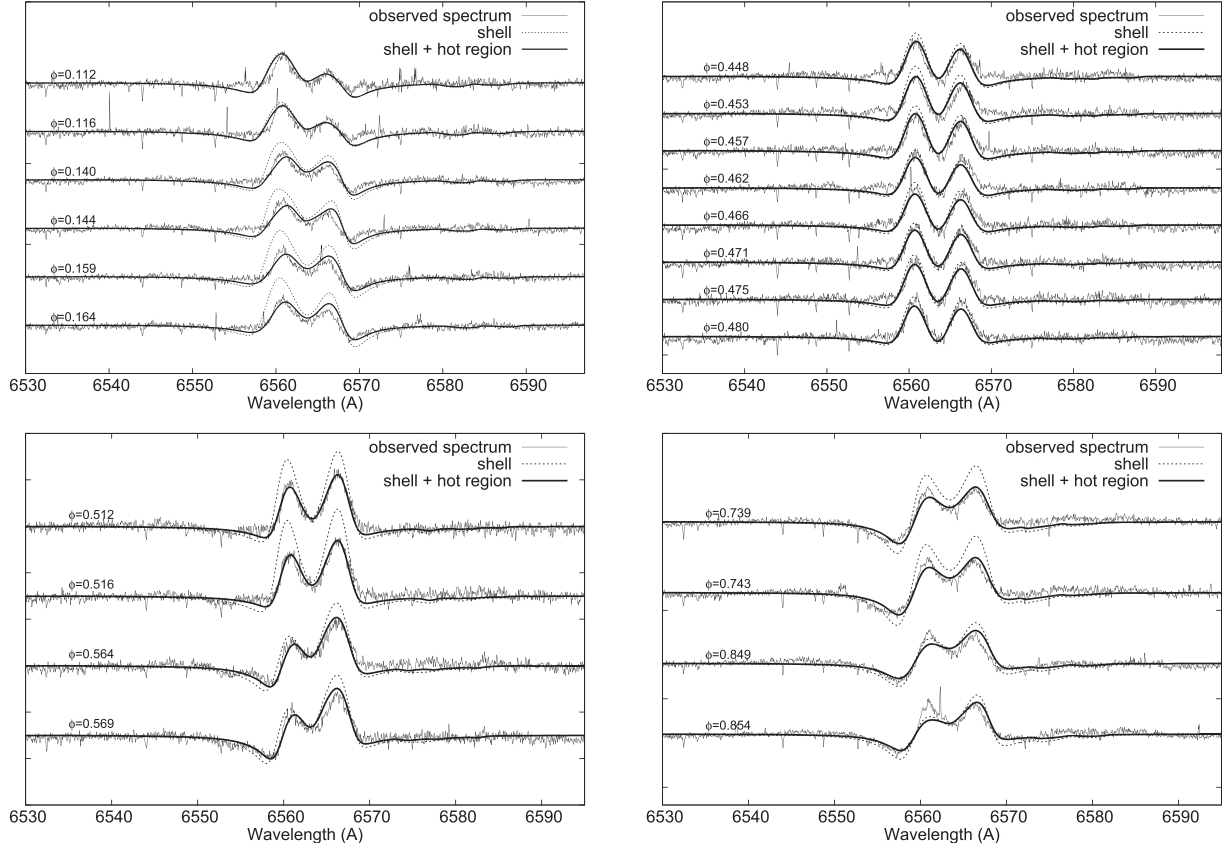
Figure 7. Shell and shell + hotspot modelling of the hydrogen line for HH Car. On the left side of the figure are shown phases when the spectra are taken.

Table 8. The model parameters obtained for the shell and hotspot region.

Parameter	Values
Shell	
T (K)	$22\,000 \pm 3000$
$R_{\text{in}}/R_{\text{out}}$ ($R_\odot$)	$27.8 \pm 1.3, 32.2 \pm 2.2$
v_{turb} (km s^{-1})	62.5 ± 7.5
v_{shell} (km s^{-1})	192.5 ± 7.5
ρ (g cm^{-3})	$(2.2 \pm 0.7) \times 10^{-13}$
Hotspot region	
T (K)	$100\,000 \pm 5000$
R ($R_\odot$)	3.2 ± 0.5
ρ (g cm^{-3})	$(90 \pm 5) \times 10^{-9}$

component was determined to be $v \sin i = 220 \pm 30$ km s^{-1}, which is approximately three times faster than the synchronous rotational velocity of the component. Asynchronous fast rotation is due to the Roche lobe overflow of the donor star (secondary component), which spins up the gainer star (primary component). Similar stars exist among the early-type interacting binaries, showing strong emission in their spectra. Thus, de Mink, Langer & Izzard (2011) state that the binary interaction can lead to a significant increase in stellar rotation rates.

For the secondary component, parameters such as temperature, surface gravity, and rotation velocity were obtained from the atmosphere models. The rotational velocity ($V_{\text{rot}} = 150$ km s^{-1}) of the secondary indicates that it is synchronized within the limits of uncertainties.

The component temperatures (33 500 K, 27 500 K) from the model atmosphere solution were also obtained from the simultaneous solution of light and radial velocity curves. The temperatures from two different methods are consistent within the limits of the errors. For this reason, it was determined that the spectral types of the components of HH Car are O9 V + B0 III–IV based on the atmosphere models. The fact that the secondary (less massive) component is left off the main sequence indicates that it was more massive in the past. Although the system is young, it can be said that after rapid mass transfer, the secondary component has reached its current less massive position. However, in order to reliably determine the mass-transfer or mass-loss rate, we need to carry out an orbital period analysis of the system. As there are currently no times of minimum observation of the system over many years, it does not seem possible to do this.

There are stellar winds and mass loss from the system in addition to mass transfer from the less massive component to the more massive component. Strong emission in the spectrum of the system is important in terms of showing the presence of the material around the components and allowing them to be studied. The composed spectra of the system (primary and secondary components, gas flow, shell and hotspot) were modelled with the SHELLSPEC program to determine the accretion disc parameters such as the gas flow and hotspot. As a result, HH Car was modelled to have a shell with a low-density gas flow from the secondary component to the primary component, a hot zone formed by the collision of stellar wind between the two components and an inhomogeneous structure surrounding the system. In particular, it would be important to examine the region with X-ray observations, where the winds of the two stars collide with
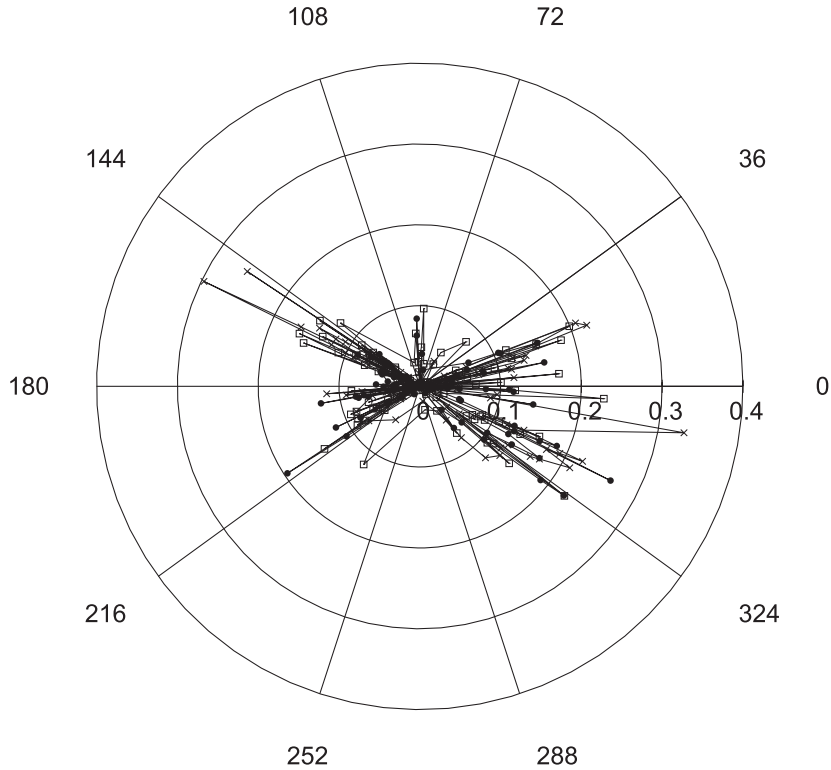
Figure 8. Distribution of the circumstellar material surrounding the components in terms of geometric length (au) using *U* (filled circle), *B* (cross) and *V* (empty square) light curves.

the flowing material. Moreover, times of minimum observations are important to monitor the orbital period changes, so that the mass-transfer and mass-loss rates can be determined. Here, we can make an estimation of the mass-loss rate of the components using the correlation between the mass-loss rate and the source luminosity (Faber & Gallagher 1976; Padovani & Matteucci 1993). They give the mass-loss rate, which is proportional to the *V*-band luminosity, as

$$\dot{M} \approx 3 \times 10^{-11} \left(\frac{L_V}{L_{\odot,V}} \right) \, M_\odot \, \mathrm{yr}^{-1}. \quad (2)$$

Using equation (2), the mass-loss rates of the componets are estimated to be $\dot{M}_1 \approx 7 \times 10^{-7}$ and $\dot{M}_2 \approx 1 \times 10^{-6}$ $M_\odot$ yr^{-1} for the primary and secondary components, respectively.

Recently, Pozo Nuñez et al. (2019) conducted a study on binary stars that covers high-massive binaries. In this study, they analysed 35 massive binary stars that they had just discovered among the massive variable stars (260) in the SIMBAD data base. It is very interesting that these systems do not include HH Car. However, the list of these massive systems gives very important clues about systems such as HH Car. For example, 14 of the systems in the list prepared by Pozo Nuñez et al. (2019) are detached, 12 of them are semidetached and seven of them are in near-contact status. This shows us that semidetached systems such as HH Car are very common among such systems.

The present study has revealed that the orbit of HH Car is circular. Apart from Zahn (1977), a more recent study by Hurley, Tout & Pols (2002) has shown that the circularization among these systems is a consequence of the short orbital periods because tidal forces will circularize the orbit before Roche lobe overflow. Moreover, all systems studied by Pozo Nuñez et al. (2019) exhibit circular orbits.

Another remarkable point mentioned in the study is the fact that O-type binary stars have the most multiple components among other binary star types. Although we do not have definitive evidence of the physical connection of the optical component of HH Car, HH Car appears to be located in a dense population of stars (see Figure 1). This is in agreement with the multiplicity characteristic of O-type binary systems.

DATA AVAILABILITY

The data underlying this article are available upon request from the corresponding author.

REFERENCES

Andersen J., 1991, A&AR, 3, 91
Andersen J., Clausen J. V., Nordstrom B., 1980, in Plavec M. J., Popper D. M., Ulrich R. K., eds, Proc. IAU Symp. Vol. 88, Close Binary Stars: Observations and Interpretation. Kluwer, Dordrecht, p. 81
Bailer-Jones C. A. L., Rybizki J., Fouesneau M., Mantelet G., Andrae R., 2018, AJ, 156, 58
Bakış V., Budding E., Erdem A., Bakış H., Demircan O., Hadrava P., 2006, MNRAS, 370, 1935

Bakış V., Hensberge H., Demircan O., Zejda M., Bilir S., Nitschelm C., 2015, in Rucinski S. M., Torres G., Zejda M., eds, ASP Conf. Ser. Vol. 496, Living Together: Planets, Host Stars and Binaries. Astron. Soc. Pac., San Francisco, CA, p. 189

Bakış V., Bakış H., Bilir S., Eker Z., 2016a, PASA, 33, e046

Bakış H., Bakış V., Eker Z., Demircan O., 2016b, MNRAS, 458, 508

Budaj J., Richards M. T., 2004, Contributions of the Astronomical Observatory Skalnate Pleso, 34, 167

Budaj J., Richards M. T., Miller B., 2005, ApJ, 623, 411

Budding E., Demircan O., 2007, Introduction to Astronomical Photometry, Vol. 6. Cambridge Univ. Press, Cambridge

Caballero J. A., 2008, MNRAS, 383, 750

Claret A., 2000, A&A, 363, 1081

Cutri R. M. et al., 2003, VizieR Online Data Catalog, II/246

de Mink S. E., Langer N., Izzard R. G., 2011, in Neiner C., Wade G., Meynet G., Peters G., eds, Proc. IAU Symp. Vol. S272, Active OB Stars: Structure, Evolution, Mass Loss, and Critical Limits. Cambridge Univ. Press, Cambridge, p. 531

Faber S. M., Gallagher J. S., 1976, Lick Observatory Bulletin, 709, 1

Gaia Collaboration, 2018, VizieR Online Data Catalog, I/345

Gray R. O., Corbally, Christopher J., 2009, Stellar Spectral Classification. Princeton Univ. Press, Princeton, NJ

Hadrava P., 2004, Publications of the Astronomical Institute of the Czechoslovak Academy of Sciences, 92, 15

Hilditch R. W., 1973, MNRAS, 164, 101

Hilditch R. W., Bell S. A., 1987, MNRAS, 229, 529

Hurley J. R., Tout C. A., Pols O. R., 2002, MNRAS, 329, 897

Ibanoğlu C., Soydugan F., Soydugan E., Dervişoğlu A., 2006, MNRAS, 373, 435

Johnson H. L., Morgan W. W., 1953, ApJ, 117, 313

Johnson D. R. H., Soderblom D. R., 1987, AJ, 93, 864

Kaitchuck R. H., Honeycutt R. K., 1982, ApJ, 258, 224

Kaufer A., Stahl O., Tubbesing S., Nørregaard P., Avila G., Francois P., Pasquini L., Pizzella A., 1999, The Messenger, 95, 8

Kreiner J. M., 2004, Acta Astron., 54, 207

Lanz T., Hubeny I., 2003, ApJS, 146, 417

Loden L. O., Sundman A., 1972, A&A, 20, 49

Lubow S. H., Shu F. H., 1975, ApJ, 198, 383

Mandrini C. H., Mendez R. H., Ferrer O. E., Niemela V. S., 1985, Rev. Mex. Astron. Astrofis., 11, 99

Mayer P., Lorenz R., Drechsel H., 1997, A&A, 320, 109

Mayer P., Drechsel H., Irrgang A., 2014, A&A, 565, A86

Mel'Nik A. M., Dambis A. K., 2009, MNRAS, 400, 518

Mel'Nik A. M., Efremov Y. N., 1995, Astron. Lett., 21, 10

Nelder J. A., Mead R., 1965, The Computer Journal, 7, 308

Nemravová J. et al., 2010, A&A, 516, A80

O'Connell D. J. K., 1968, Ricerche Astronomiche, 7, 399

Owocki S. P., Rybicki G. B., 1984, ApJ, 284, 337

Özkardeş B., Erdem A., Bakış V., 2009, New Astron., 14, 461

Padovani P., Matteucci F., 1993, ApJ, 416, 26

Peters G. J., 1989, Space Sci. Rev., 50, 9

Petrenz P., Puls J., 1996, A&A, 312, 195

Petrie R. M., Andrews D. H., Scarfe C. D., 1967, in Batten A. H., Heard J. F., eds, Proc. IAU Symp. Vol. 30, Determination of Radial Velocities and their Applications. Kluwer, Dordrecht, p. 221

Popper D. M., 1980, ARA&A, 18, 115

Pozo Nuñez F., Chini R., Barr Domínguez A., Fein C., Hackstein M., Pietrzyński G., Murphy M., 2019, MNRAS, 490, 5147

Richards M. T., Albright G. E., 1999, ApJS, 123, 537

Richardson N. D., Gies D. R., Henry T. J., Fernández-Lajús E., Okazaki A. T., 2010, AJ, 139, 1534

Silaj J., Jones C. E., Tycner C., Sigut T. A. A., Smith A. D., 2010, ApJS, 187, 228

Soderhjelm S., 1975, A&AS, 22, 263

Stevens I. R., Blondin J. M., Pollock A. M. T., 1992, ApJ, 386, 265

Straizys V., Kuriliene G., 1981, Ap&SS, 80, 353

Tatum J. B., 1968, MNRAS, 141, 43

Tetzlaff N., Neuhäuser R., Hohle M. M., Maciejewski G., 2010, MNRAS, 402, 2369

Thaller M. L., 1997, ApJ, 487, 380

Vanbeveren D., Mennekens N., 2017, in Miroshnichenko A.et al., eds, The B[e] Phenomenon: Forty Years of Studies, ASP Conf. Ser. Vol. 508. Astron. Soc. Pac., San Francisco, CA, p. 121

Wilson R. E., 2008, ApJ, 672, 575

Worthey G., Lee H-c., 2011, ApJS, 193, 1

Zahn J.-P., 1977, A&A, 57, 383

This paper has been typeset from a TEX/LATEX file prepared by the author.